Ligand-Induced Differences in Secondary Structure of the *Vibrio parahaemolyticus* Na^+/Galactose Cotransporter†

Johannes le Coutre,*,‡ Eric Turk,§ H. Ronald Kaback,|| and Ernest M. Wright*,§

Nestlé Research Center, 1000 Lausanne 26, Switzerland, and Departments of Physiology and Howard Hughes Medical Institute, Departments of Physiology and of Microbiology, Immunology, and Molecular Genetics, and Molecular Biology Institute, University of California, Los Angeles, California 90095

Received February 22, 2002; Revised Manuscript Received April 25, 2002

ABSTRACT: A detailed structural study of the prokaryotic sodium/galactose transporter (vSGLT) from *Vibrio parahaemolyticus* using attenuated total reflection Fourier transform infrared (ATR-FTIR) spectroscopy reveals stepwise increases in α-helicity upon binding of sodium and D-galactose. These increases in helicity correlate with decreases in β-structural elements. The changes are accompanied by stepwise reductions in the degree of H/D exchange (HDX), suggesting reduced accessibility of water to the protein backbone. The data demonstrate discrete conformational changes from one intermediate to the next during the catalytic cycle of the protein and are interpreted in a model of the symport reaction mechanism.

Understanding structure/function relationships on the atomic level in a membrane transport protein during turnover remains an enigma due to the scarce availability of structural information on this class of proteins. However, it is evident that conformational changes are key events in the catalytic cycle of membrane transport proteins since the accessibility and/or affinity for coupling ion(s) and substrate molecule(s) may change during translocation from one side of the membrane to the other (*1*). Membrane symport proteins of the Na^+-coupled cotransporter family SGLT occur in Bacteria, Archaea, and Eukarya. Both in the prokaryotic cytoplasmic membrane and in eukaryotic epithelial membranes these molecules are involved in the uptake of nutrients such as sugars and amino acids and anions such as pantothenate, biotin, and iodide. A kinetic model has been proposed for the catalytic cycle of human SGLT1 suggesting the sequential binding of first sodium and second the sugar to the outward-oriented protein, eliciting a conformational change that results in an inward presentation of the substrates, followed by the cytoplasmic release of sugar and sodium (*2*).

To overcome impediments related to the study of eukaryotic membrane proteins such as overexpression, trafficking, and posttranslational modification, a prokaryotic relative—vSGLT from *Vibrio parahaemolyticus*—has been established as a paradigm for Na^+-coupled sugar transport. vSGLT has been cloned, overexpressed, and purified, and the protein has been reconstituted into proteoliposomes where it is active as a monomer (*3*−*8*). Binding and release of substrate trigger specific conformational changes that propel the catalytic cycle of membrane transport proteins from one intermediate to the next. For vSGLT in the lipid-reconstituted system, the affinities for Na^+ and galactose (K_{Na} ∼130 mM in 100 μM galactose and $K_{galactose}$ ∼160 μM in 100 mM Na^+) are comparable to those measured for the mammalian cotransporters (*5*, *6*).

This study focuses on the binding of sodium and galactose to vSGLT by using a sodium/potassium replacement strategy for the direct study of sodium binding on the same sample mounted in the FTIR spectrometer.

MATERIALS AND METHODS

Protein and Sample Preparation. vSGLT was purified as described in (*6*) using a pBAD18 vector, a 10 residue C-terminal linker, and a hexa-His affinity tag for purification. The purified protein (1500 μg) was incorporated into lipid bilayers of soy lecithin/cholesterol, 9:1, using a lipid-to-protein ratio of 6.4:1, w/w (*6*), since this lipid composition had been found to elicit the highest Na^+-dependent D-galactose transport activity. A 50 mM $(K,H)_3PO_4$ buffer (pH 7.0), with the specified solutes, was used throughout this study; KOH restored the pH to 7.0 upon addition of NaCl to 150 mM. For FTIR spectroscopy, the sample (240 μL; ca. 430 μg of vSGLT) was dried on a germanium internal reflection element (25 reflections), washed with the specified substrate in phosphate buffer, and dried again, from a smaller volume, to minimize the increase in [solutes] in the film. The protein retained transport activity as judged by uptake assays after the FTIR experiments where the proteoliposomes were recovered from the surface of the crystal, hydrated, and dispersed by sonication.

IR Spectroscopy. IR spectra were collected on a BOMEM-DA3 FTIR spectrometer purged with N_2. Typically, interferograms were recorded with 4 cm^{-1} spectral resolution and

† This research was supported by NIH Grants DK44582, DK51131, and DK44602.

* Correspondence should be addressed to either of these authors. J.C.: Nestlé Research Center Lausanne, Vers-Chez-Les-Blanc, 1000 Lausanne 26, Switzerland; phone: +(41/21) 785 8686, fax: +(41/21) 785 8549, email: johannes.le-coutre@rdls.nestle.com. E.M.W.: Department of Physiology, University of California Los Angeles School of Medicine, Los Angeles, CA 90095-1751; phone: (310) 825 6905, email: ewright@mednet.ucla.edu.

‡ Nestlé Research Center, Lausanne.

§ Department of Physiology, University of California, Los Angeles.

|| Howard Hughes Medical Institute, University of California, Los Angeles.

10.1021/bi025692d CCC: $22.00
Published on Web 05/29/2002

processed by using Blackman Harris apodization. A modified continuous flow ATR setup (Janos Technology, Townshend, VT) equipped with a wire grid polarizer (Harrick Scientific) was used (*9, 10*). Measurements were performed at room temperature using an incident angle of 45°, and were repeated up to 3 times. Spectra were generated by averaging 500 interferograms. For a precise secondary structure analysis, synthetic spectra were generated incorporating the absorbance of parallel and perpendicular polarized light, relative to the plane of incidence, with $A_{synthetic} = A_{parallel} + (1.44 \times A_{perpendicular})$ (*11*). The semidry proteolipid film was equilibrated for 2 h in $(K,D)_3PO_4$-buffered D_2O before analysis, to eliminate the O−H bending absorbance of water which would otherwise contaminate the amide I band. All spectra were deconvoluted and fitted with a standardized procedure using Bayesian and maximum-likelihood algorithms provided by the RAZOR software for GRAMS 386. Band assignments for interpretation of the spectra are taken from (*12*) and (*13*).

Binding of Ligand. To minimize the occurrence of artifacts, sodium binding was studied online with the semidry proteolipid sample mounted in the FTIR instrument. An initial spectrum was recorded of the sample in potassium buffer equilibrated and stabilized via a constant flow of N_2 saturated with D_2O or H_2O using a flow rate of 57 L/h. Binding of sodium was induced by replacing the original potassium buffer, i.e., washing extensively with buffered 150 mM NaCl and drying the mounted sample with D_2O- or H_2O-saturated nitrogen gas, respectively. The addition of sugar to the film may induce changes in the overall IR signal due to a different degree of hydration caused by hygroscopic swelling of the film, which is negligible in the case of sodium. Therefore, to study the effect of 150 μM D-galactose (or L-glucose), a new sample preincubated with the specified sugar was used.

H/D Exchange. Semidry proteolipid films were equilibrated under H_2O-saturated nitrogen flow until the difference between two subsequently recorded spectra showed no significant bands especially in the amide I region. At $t = 0$, the N_2 flow was switched from H_2O to D_2O vapor, and spectra were recorded initially with 10 and subsequently with up to 1000 co-added scans. Time points for HDX[1] curves were then assigned to the midpoint of the time interval needed to record one spectrum. The integral intensity of the amide II band was normalized to the lipid C=O stretching vibration (1765−1705 cm^{-1}), and the intensity of the last spectrum recorded prior to deuteration was set to 100% H_2O.

RESULTS

Secondary Structure of vSGLT. Three experimental conditions were used to stabilize different intermediates of the vSGLT catalytic cycle: (1) a ligand-free form in potassium buffer to compensate for salt effects or osmotic effects; (2) a sodium-bound form; and (3) a (sodium + D-galactose)-bound form (Figure 1). As a control for the latter condition, we also recorded the spectrum in sodium + L-glucose. The measured amide I regions are reproduced well using a band fit of six components that represent similar bands in each of the three spectra. Only the amide I spectrum of the sample in potassium (prior to the binding of sodium) requires one additional component at 1603 cm^{-1} which clearly improves

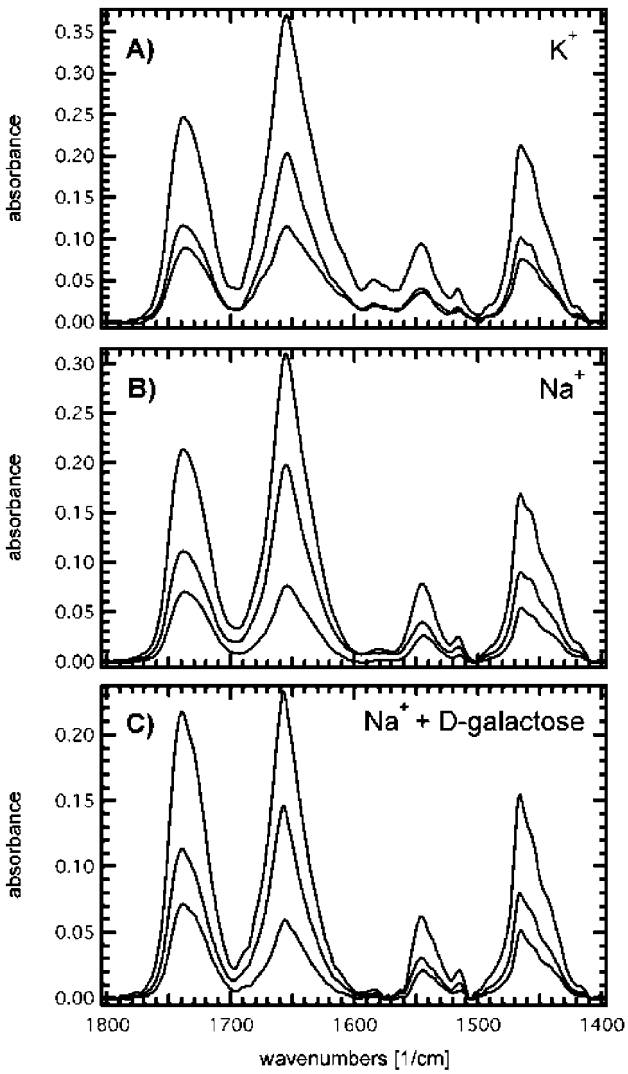

FIGURE 1: Polarized FTIR absorbance spectra of vSGLT reconstituted into a lecithin/cholesterol bilayer and recorded in deuterated buffer. In each panel, the bottom trace represents the spectrum recorded with perpendicular polarized light, the middle trace is recorded with parallel polarized light, and the top trace is calculated using: $A_{synthetic} = A_{parallel} + (1.44 \times A_{perpendicular})$ (*11*). (A) Spectra representing the ligand-free protein in potassium buffer. (B) Spectra measured on the same sample as in (A) upon exposure to 150 mM sodium. (C) Spectra of a new sample preincubated with D-galactose to yield a final concentration of 150 μM in the semidry film.

the fit and might reflect extended β structures (Figure 2, Table 1) (*13*). The deconvoluted and fitted spectra are dominated by a spectral component at 1656 cm^{-1} indicating a large amount of α-helix. Interestingly, upon binding of sodium and subsequently of galactose, the relative amount of α-helix increases each time about 10%, corresponding to approximately 56 amino acids that are incorporated into α-helical structures (10% of 558, i.e., total number of vSGLT peptide bonds). In turn, the relative intensity of bands at 1670 and 1630 cm^{-1}, indicating the contribution of β-sheet- and β-turn-like structural elements, decreases with the sequential binding of sodium and galactose. A band at 1640−1643 cm^{-1} is indicative of random coil, and even though it contributes 20−25% relative intensity, it clearly is not as affected by the induced changes of ligand. The effect of D-galactose on the secondary structure was specific since the spectrum in

[1] Abbreviation: HDX, hydrogen/deuterium exchange.

Table 1: Influence of Ligands on the Secondary Structure of vSGLT[a]

	β-sheet	β-turns	α-helix	random coil	β-sheet	β or extended structures	
(A) no ligand (potassium)	1683	1672	1656	1643	1629	1613	1603
	1 ± 1%	17 ± 2%	35 ± 3%	21 ± 6%	19 ± 7%	5 ± 4%	2 ± 1%
(B) sodium	1681	1669	1656	1642	1628	1615	
	3 ± 2%	13 ± 5%	45 ± 10%	26 ± 6%	10 ± 4%	3 ± 1%	
(C) sodium + L-glucose	1683	1669	1657	1642	1625	1612	
	3 ± 3%	14 ± 10%	45 ± 13%	27 ± 10%	9 ± 5%	1 ± 1%	
(D) sodium + D-galactose	1690	1674	1658	1643	1629	1611	
	3 ± 0.5%	11 ± 1%	53 ± 2%	21 ± 3%	10 ± 2%	2 ± 1%	

[a] The synthetic amide I spectra for the experiment shown in Figure 2 were deconvoluted and fitted as described under Materials and Methods. Each band is characterized by its wavenumber (cm^{-1}), by its contribution to the total amide I spectrum, and by the confidence limits derived by the band fitting procedure method. The secondary structure predictions are shown in (A) the absence of ligand (potassium), (B) the presence of sodium, (C) the presence of sodium and L-glucose, and (D) the presence of sodium and D-galactose.

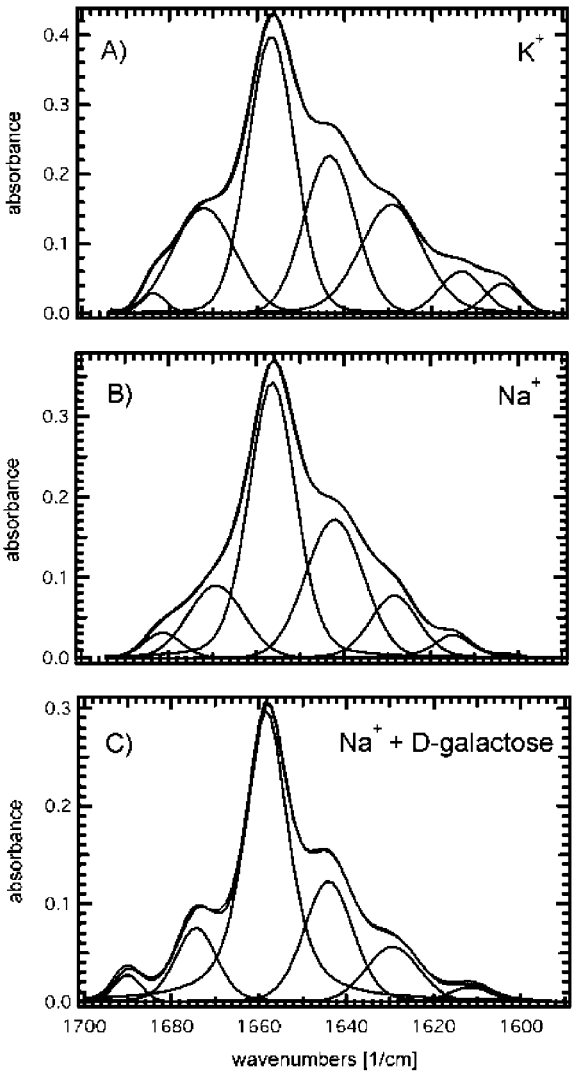

FIGURE 2: Deconvoluted and fitted amide I bands of the synthetic spectra corresponding to the experimental conditions described in Figure 1 (for explanation and assignments, also see Table 1).

the presence of sodium and L-glucose was identical to that in sodium alone (Table 1).

Orientation of the Protein. An increase in the dichroic ratio (R^{ATR}) of the amide I band occurs upon addition of 150 mM sodium from 1.77 to 2.46 as measured by the integral intensity of the amide I band between 1660 and 1690 cm^{-1}. Such changes and their relation to the average α-helical tilt angle of a membrane protein are discussed controversially

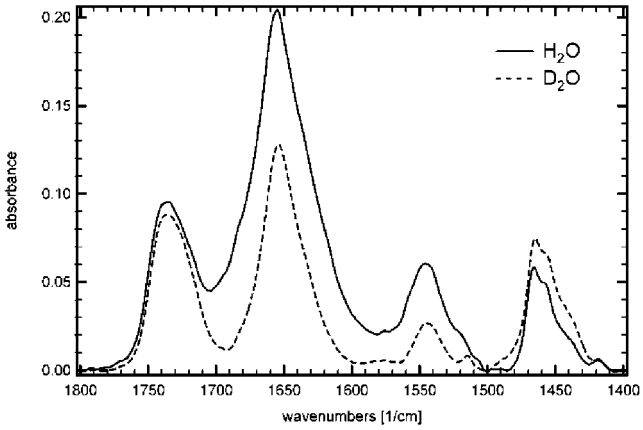

FIGURE 3: FTIR absorbance spectrum of vSGLT in H_2O potassium buffer (top trace) and in D_2O potassium buffer (bottom trace). The decrease in intensity of the "amide I" band at 1656 cm^{-1} is due to loss of the water OH-bending vibration. In contrast, the amide II band at 1545 cm^{-1} is indicative of the peptide backbone NH-bending mode that shifts to 1455 cm^{-1} upon H/D exchange (peptide backbone ND-bending).

in the literature (*14*, *15*) and certainly depend on the axiality of the protein which is not known for vSGLT. Nevertheless, the observed increase in R^{ATR} is indicative of a decrease in the average α-helical tilt angle with respect to the membrane normal upon addition of sodium.

H/D Exchange. To study the effects of HDX in proteins, the amide II band at 1550 cm^{-1} is a useful indicator. In the hydrated form, this band is indicative of the amide N−H bending mode of all backbone peptide bonds. HDX shifts this absorption to lower frequencies at about 1450 cm^{-1}, leaving only that amount of intensity at the original frequency which corresponds to non-H/D-exchanged backbone amide groups. The decrease of the amide II band and the corresponding increase of the band at 1450 cm^{-1} (Figure 3) are accompanied by decreased intensity of the lipid C═O stretching vibration at 1730 cm^{-1} caused by swelling of the sample, which is therefore used to normalize the amide II band.

The time courses recorded on HDX of vSGLT confirm three distinct intermediate structures (Figure 4). Quickly exchanging amide protons are fully deuterated after about 2 h, and the sample without ligand shows the highest degree of approximately 50% exchange. Addition of sodium reduces the overall degree of exchange by about 5%, and addition of galactose to the sodium-bound form reduces total HDX by another 5%. To verify the effects of galactose, an

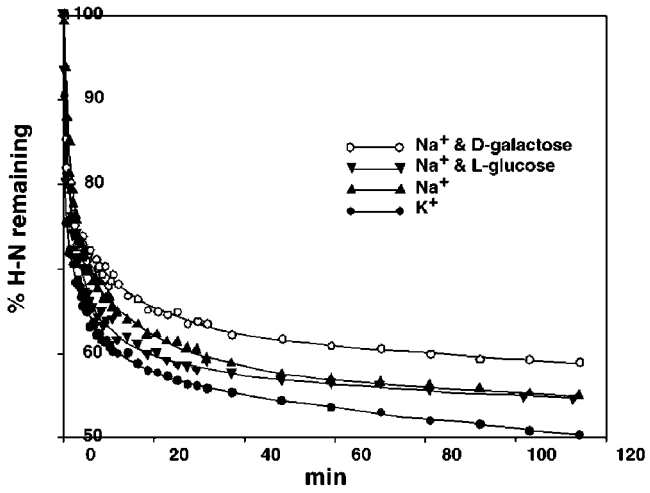

FIGURE 4: Time course of H/D exchange for vSGLT. Equilibration in sodium buffer (▲) after recording of an initial time course in potassium buffer (●) leads to a 5% reduction in total hydrogen deuterium exchange (HDX). Another 5% reduction in HDX is observed upon equilibrating the proteolipid film in a buffer containing sodium and D-galactose (○). Equilibration in sodium buffer with L-glucose as a negative control (▼) does not yield the same degree of HDX (for details, see text).

important control has been performed by the addition of L-glucose instead of D-galactose. L-Glucose is not transported by vSGLT (*6*), and in the presence of Na^+, it does not alter the total degree of exchange (Figure 4). Multiexponential curve fitting of the time courses required a minimum of four terms (half-lives), indicating the broad range of time constants characterizing the solvent accessibilities of the backbone protons.

DISCUSSION

The key intermediates of the vSGLT catalytic cycle were stabilized and then characterized using polarized ATR-FTIR spectroscopy and HDX experiments. Relative spectral changes display the critical features of the transport mechanism, and the spectra were analyzed carefully with respect to absolute quantification of secondary structure because unknown side chains contribute to the amide I envelope (*16*). An α-helical content ranging from 35% to 53% (Table 1), depending on the presence of ligand, seems very low for a protein with 559 amino acids that spans the membrane with 14 segments. Therefore, one or several stretched β-structured elements or very short α-helices have to be assumed. A possible candidate for this would be transmembrane segment 2. This domain is striking throughout the SGLT family of cotransporters for its rather low hydrophobicity, peculiar abundance of small amino acid residues (Gly, Ala, and Ser), and ambiguous helix/loop boundaries (*17, 18*).

The total amount of α-helix increases with the binding of each ligand at the cost of β-structural elements. Increases in helix content are accompanied by decreases in the average α-helical tilt angle. Similar secondary structure changes accompanying the binding of a ligand have been observed with elongation factor Tu, where an α-helix melts on one end and grows on the other end together with a tilting movement upon changing from the inactive GDP-bound form to the active GTP-bound form (*19, 20*).

Studying the time courses of hydrogen/deuterium exchange reveals not only the total degree of water accessibility but also the presence of individual protein domains with different accessibilities. The profiles of the HDX time courses for vSGLT do not display the extreme degree of H/D exchange that has been found for other membrane transport proteins such as the *E. coli* lactose permease (*10, 21*) or the human erythrocyte glucose transporter (*22*). Instead, the time course profiles are more similar to those found for the potassium channel KcsA (*9*). This difference in HDX between vSGLT and lactose permease might be due to several reasons: (1) The coupling ion in the permease is a proton versus Na^+ in vSGLT, and thus widespread intramolecular H-bonded networks might exist in the permease that facilitate deuteration of the backbone (*23*). (2) Lactose as a disaccharide might require more hydrophilicity in a membrane translocation pathway compared to galactose as a monosaccharide.

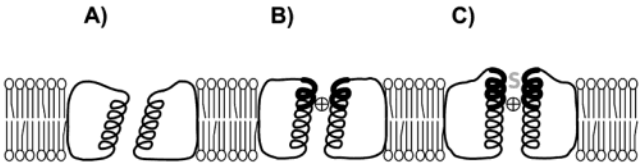

FIGURE 5: Schematic model describing changes in vSGLT secondary structure upon binding of sodium and galactose (for details, see text). (A) Ligand-free protein in potassium buffer. (B) Sodium-bound form. (C) Translocation-competent configuration with bound sodium and D-galactose.

Based upon the spectroscopic observations, a model is proposed to explain the binding of sodium and galactose to vSGLT (Figure 5). Binding of sodium leads to an increase in α-helicity through the recruitment of loose β-sheet and β-turn secondary structural elements, which "solidify" to build a well-defined binding site. Whereas the number of helices involved remains unknown (sodium binding might affect 1 or several helices), it can be estimated that about 28 residues are involved in the sodium-induced rearrangement (5% of 558 peptide bonds). For coordination of the sodium cation, residues with a negative or a partial negative charge might be involved, and it is even feasible that backbone carbonyl groups participate in the binding. The binding of sodium primes the protein to configure a provisional binding site for galactose in a similar fashion. The subsequent binding of galactose induces a final increase in α-helicity (another 5%, or about 28 residues), which shifts the protein into a translocation-competent configuration for substrate transport. It is unknown whether the induced α-helical segments directly contact the substrates or not. For the *E. coli* lactose permease, the lactose binding site has been described to be located between helices IV and V and stabilized by an intrahelical Glu/Arg salt bridge where one free amino group of the Arg guanidino function holds the galactose moiety of lactose in place (*24*−*28*).

The decreases in HDX as induced by substrate binding may be due either to the recruitment of β-sheets and -turns into more compact α-helical segments, or to an increased rigidity of the protein, or to both. Since the change in water accessibility as derived from the HDX experiments amounts to half the number of residues that are involved in de novo α-helix formation, it is intriguing to speculate that possibly neighboring α-helical elements are extended to embrace the ligands as a binding site (i.e., induced fit). Only one side of each helical extension is exposed to the ligand whereas the other side faces hydrophobic areas of either membrane lipids or further helices where no HDX will occur.

In summary, three effects that are observable by ATR-FTIR, and are mutually consistent, accompany the binding of substrates to vSGLT. Sodium and galactose incrementally increase the α-helical content at the cost of β-sheet and β-turn, decrease the average transmembrane helix tilt angle, and increase the resistance of backbone protons to deuterium exchange. The first two effects are expected, on simple geometrical grounds, to result in a compaction of the overall protein structure in the membrane. The increased resistance to deuterium exchange is consistent with and supportive of this ligand-induced protein compaction, and is also suggestive of a ligand-induced rigidification of structure.

ACKNOWLEDGMENT

We thank Miranda Rizk and Marloes Veenstra for technical assistance and Dr. C. Kumar N. Patel for use of the FTIR spectrometer.

REFERENCES

1. le Coutre, J., and Kaback, H. R. (2001) *Biopolym.: Pept. Sci. 55*, 297−307.
2. Loo, D. D., Hirayama, B. A., Gallardo, E. M., Lam, J. T., Turk, E., and Wright, E. M. (1998) *Proc. Natl. Acad. Sci. U.S.A. 95*, 7789−7794.
3. Sarker, R. I., Ogawa, W., Shimamoto, T., Shimamoto, T., and Tsuchiya, T. (1997) *J. Bacteriol. 179*, 1805−1808.
4. Sarker, R. I., Okabe, Y., Tsuda, M., and Tsuchiya, T. (1996) *Biochim. Biophys. Acta 1281*, 1−4.
5. Sarker, R. I., Ogawa, W., Tsuda, M., Tanaka, S., and Tsuchiya, T. (1996) *Biochim. Biophys. Acta 1279*, 149−156.
6. Turk, E., Kim, O., le Coutre, J., Whitelegge, J. P., Eskandari, S., Lam, J. T., Kreman, M., Zampighi, G., Faull, K. F., and Wright, E. M. (2000) *J. Biol. Chem. 275*, 25711−25716.
7. le Coutre, J., Whitelegge, J. P., Gross, A., Turk, E., Wright, E. M., Kaback, H. R., and Faull, K. F. (2000) *Biochemistry 39*, 4237−4242.
8. Xie, Z., Turk, E., and Wright, E. M. (2000) *J. Biol. Chem. 275*, 25959−25964.
9. le Coutre, J., Kaback, H. R., Patel, C. K., Heginbotham, L., and Miller, C. (1998) *Proc. Natl. Acad. Sci. U.S.A. 95*, 6114−6117.
10. le Coutre, J., Narasimhan, L. R., Patel, C. K., and Kaback, H. R. (1997) *Proc. Natl. Acad. Sci. U.S.A. 94*, 10167−10171.
11. Marsh, D. (1999) *Biophys. J. 77*, 2630−2637.
12. Byler, D. M., and Susi, H. (1986) *Biopolymers 25*, 469−487.
13. Goormaghtigh, E., Cabiaux, V., and Ruysschaert, J. M. (1994) *Subcell. Biochem. 23*, 405−450.
14. Citra, M. J., and Axelsen, P. H. (1996) *Biophys. J. 71*, 1796−1805.
15. Marsh, D. (1998) *Biophys. J. 75*, 354−358.
16. Jackson, M., and Mantsch, H. H. (1995) *Crit. Rev. Biochem. Mol. Biol. 30*, 95−120.
17. Turk, E., and Wright, E. M. (1997) *J. Membr. Biol. 159*, 1−20.
18. Turk, E., Kerner, C. J., Lostao, M. P., and Wright, E. M. (1996) *J. Biol. Chem. 271*, 1925−1934.
19. Berchtold, H., Reshetnikova, L., Reiser, C. O., Schirmer, N. K., Sprinzl, M., and Hilgenfeld, R. (1993) *Nature 365*, 126−132.
20. Sprinzl, M. (1994) *Trends Biochem. Sci. 19*, 245−250.
21. Patzlaff, J. S., Moeller, J. A., Barry, B. A., and Brooker, R. J. (1998) *Biochemistry 37*, 15363−15375.
22. Alvarez, J., Lee, D. C., Baldwin, S. A., and Chapman, D. (1987) *J. Biol. Chem. 262*, 3502−3509.
23. le Coutre, J., Tittor, J., Oesterhelt, D., and Gerwert, K. (1995) *Proc. Natl. Acad. Sci. U.S.A. 92*, 4962−4966.
24. Sahin-Toth, M., le Coutre, J., Kharabi, D., le Maire, G., Lee, J. C., and Kaback, H. R. (1999) *Biochemistry 38*, 813−819.
25. Frillingos, S., Sahin-Toth, M., Wu, J., and Kaback, H. R. (1998) *FASEB J. 12*, 1281−1299.
26. Venkatesan, P., and Kaback, H. R. (1998) *Proc. Natl. Acad. Sci. U.S.A. 95*, 9802−9807.
27. Frillingos, S., Gonzalez, A., and Kaback, H. R. (1997) *Biochemistry 36*, 14284−14290.
28. Guan, L., Sahin-Toth, M., and Kaback, H. R. (2002) *Proc. Natl. Acad. Sci. U.S.A. 99*, 6613−6618.

BI025692D